ECMWF COPERNICUS REPORT

Copernicus Climate Change Service

Algorithm Theoretical Basis Document (ATBD) – ANNEX B for products CO2_GO2_SRFP & CH4_GO2_SRFP (v2.0.0, 2019-2022)

C3S2_312a_Lot2_DLR – Atmosphere

Issued by: Andrew Barr and Tobias Borsdorff, SRON, The Netherlands

Date: 06/02/2024

Ref: C3S2_312a_Lot2_D-WP1_ATBD-2023-GHG_ANNEX-B_v7.1b

Official reference number service contract: 2021/C3S2_312a_Lot2_DLR/SC1

PROGRAMME OF THE EUROPEAN UNION

IMPLEMENTED BY ECMWF

Contributors

INSTITUTE OF ENVIRONMENTAL PHYSICS (IUP), UNIVERSITY OF BREMEN, BREMEN, GERMANY
(IUP)
M. Buchwitz

SRON NETHERLANDS INSTITUTE FOR SPACE RESEARCH, LEIDEN, THE NETHERLANDS
(SRON)
T. Borsdorff
A. G. Barr
O. P. Hasekamp

History of modifications

Version	Date	Description of modification	Chapters / Sections
1.1	20-October-2017	New document for data set CDR1 (2009-2016)	All
2.0	4-October-2018	Update for CDR2 (2009-2017)	All
3.0	12-August-2019	Update for CDR3 (2009-2018)	All
3.1	03-November-2019	Update after review by Assimila: Primarily correction of typos and broken links. Some additional explanations added.	All
4.0	18-August-2020	Update for CDR4 (2009-2019)	All
5.0	18-February-2021	Update for CDR5 (2009-mid2020)	All
6.0 Draft	18-February-2022	Update for data set CDR6: First draft	All
6.0	4-August-2022	Update for CDR6: GOSAT-2 retrievals (2019 - 2021)	All
6.1	25-November-2022	Update after review (use of new template, various mostly minor improvements at several places)	All
6.2	31-January-2023	Minor improvements at various places taking into account feedback from 2nd review	All
7.0 (Draft 1)	23-February-2023	Initial draft for data set CDR7	All
7.0 (Draft 2)	27-April-2023	Improvements based on review	All
7.0 (Draft 3)	29-June-2023	Improvements based on independent review	All
7.0 (Draft 4)	03-August-2023	Improved Draft after review	All
7.0	28-August-2023	Minor improvements at various places	All
7.1	13-September-2023	Minor improvements after review	All
7.1b (beta)	1-February-2024	Minor improvements after review	All
7.1b	6-February-2024	Typo corrected after review	Page 37

List of datasets covered by this document

Deliverable ID	Product title	Product type (CDR, ICDR)	Version number	Delivery date
WP2-FDDP-GHG-v2	CO2_GO2_SRFP	CDR 7	2.0.0	31-Aug-2023
WP2-FDDP-GHG-v2	CH4_GO2_SRFP	CDR 7	2.0.0	31-Aug-2023

Related documents

Reference ID	Document
D1	Main ATBD: Buchwitz, M., et al., Algorithm Theoretical Basis Document (ATBD) – Main document for Greenhouse Gas (GHG: CO_2 & CH_4) data set CDR 7 (2003-2022), project C3S2_312a_Lot2_DLR – Atmosphere, ATBD v7.1, 2023. *(this document is an ANNEX to the Main ATBD)*
D2	Barr, A. G., et al., Product User Guide and Specification (PUGS) – ANNEX B for product CH4_GO2_SRFP and CO2_GO2_SRFP (v2.0.0, 2019-2021), Technical Report C3S project C3S2_312a_Lot2_DLR – Atmosphere, 2023.

Acronyms

Acronym	Definition
AIRS	Atmospheric Infrared Sounder
AMSU	Advanced Microwave Sounding Unit
ATBD	Algorithm Theoretical Basis Document
BESD	Bremen optimal EStimation DOAS
CAR	Climate Assessment Report
C3S	Copernicus Climate Change Service
CCDAS	Carbon Cycle Data Assimilation System
CCI	Climate Change Initiative
CDR	Climate Data Record
CDS	(Copernicus) Climate Data Store
CMUG	Climate Modelling User Group (of ESA's CCI)
CRG	Climate Research Group
D/B	Data base
DOAS	Differential Optical Absorption Spectroscopy
EC	European Commission
ECMWF	European Centre for Medium Range Weather Forecasting
ECV	Essential Climate Variable
EMMA	Ensemble Median Algorithm
ENVISAT	Environmental Satellite (of ESA)
EO	Earth Observation
ESA	European Space Agency
EU	European Union
EUMETSAT	European Organisation for the Exploitation of Meteorological Satellites
FCDR	Fundamental Climate Data Record
FoM	Figure of Merit
FP	Full Physics retrieval method
FTIR	Fourier Transform InfraRed
FTS	Fourier Transform Spectrometer
GCOS	Global Climate Observing System
GEO	Group on Earth Observation
GEOSS	Global Earth Observation System of Systems
GHG	GreenHouse Gas
GOS	GOSAT
GO2	GOSAT-2
GOME	Global Ozone Monitoring Experiment
GMES	Global Monitoring for Environment and Security
GOSAT	Greenhouse Gases Observing Satellite

GOSAT-2	Greenhouse Gases Observing Satellite 2
IASI	Infrared Atmospheric Sounding Interferometer
IMAP-DOAS (or IMAP)	Iterative Maximum A posteriori DOAS
IPCC	International Panel in Climate Change
IUP	Institute of Environmental Physics (IUP) of the University of Bremen, Germany
JAXA	Japan Aerospace Exploration Agency
JCGM	Joint Committee for Guides in Metrology
L1	Level 1
L2	Level 2
L3	Level 3
L4	Level 4
LMD	Laboratoire de Météorologie Dynamique
MACC	Monitoring Atmospheric Composition and Climate, EU GMES project
NA	Not applicable
NASA	National Aeronautics and Space Administration
NetCDF	Network Common Data Format
NDACC	Network for the Detection of Atmospheric Composition Change
NIES	National Institute for Environmental Studies
NIR	Near Infra Red
NLIS	LMD/CNRS *neuronal* network mid/upper tropospheric CO_2 and CH_4 retrieval algorithm
NOAA	National Oceanic and Atmospheric Administration
Obs4MIPs	Observations for Climate Model Intercomparisons
OCFP	OCO-2 Full Physics (FP) algorithm (used by Univ. Leicester)
OCO	Orbiting Carbon Observatory
OCPR	OCO-2 Proxy (PR) algorithm (used by Univ. Leicester)
OE	Optimal Estimation
PBL	Planetary Boundary Layer
ppb	Parts per billion
ppm	Parts per million
PQAD	Product Quality Assurance Document
PQAR	Product Quality Assessment Report
PR	(light path) PRoxy retrieval method
PVIR	Product Validation and Intercomparison Report
QA	Quality Assurance
QC	Quality Control
RemoTeC	Retrieval algorithm developed by SRON
REQ	Requirement
RMS	Root-Mean-Square
RTM	Radiative transfer model

SCIAMACHY	SCanning Imaging Absorption spectroMeter for Atmospheric ChartographY
SCIATRAN	SCIAMACHY radiative transfer model
SRON	SRON Netherlands Institute for Space Research
SRFP	SRON's Full Physics (FP) algorithm (also referred to a RemoTeC FP)
SRPR	SRON's Proxy (PR) algorithm (also referred to a RemoTeC PR)
SWIR	Short Wava Infra-Red
TANSO	Thermal And Near infrared Sensor for carbon Observation
TANSO-FTS	Fourier Transform Spectrometer on GOSAT
TANSO-FTS-2	Fourier Transform Spectrometer on GOSAT-2
TBC	To be confirmed
TBD	To be defined / to be determined
TCCON	Total Carbon Column Observing Network
TIR	Thermal Infra-Red
TR	Target Requirements
TRD	Target Requirements Document
WFM-DOAS (or WFMD)	Weighting Function Modified DOAS
UoL	University of Leicester, United Kingdom
URD	User Requirements Document
WMO	World Meteorological Organization
Y2Y	Year-to-year (bias variability)

General definitions

Essential climate variable (ECV)

An ECV is a physical, chemical, or biological variable or a group of linked variables that critically contributes to the characterization of Earth's climate.

Climate data record (CDR)

The US National Research Council (NRC) defines a CDR as a time series of measurements of sufficient length, consistency, and continuity to determine climate variability and change.

Fundamental climate data record (FCDR)

A fundamental climate data record (FCDR) is a CDR of calibrated and quality-controlled data designed to allow the generation of homogeneous products that are accurate and stable enough for climate monitoring.

Thematic climate data record (TCDR)

A thematic climate data record (TCDR) is a long time series of an essential climate variable (ECV).

Intermediate climate data record (ICDR)

An intermediate climate data record (ICDR) is a TCDR which undergoes regular and consistent updates, for example because it is being generated by a satellite sensor in operation.

Satellite data processing levels

The NASA Earth Observing System (EOS) distinguishes six processing levels of satellite data, ranging from Level 0 (L0) to Level 4 (L4) as follows.

L0	Unprocessed instrument data
L1A	Unprocessed instrument data alongside ancillary information
L1B	Data processed to sensor units (geo-located calibrated spectral radiance and solar irradiance)
L2	Derived geophysical variables (e.g., XCO_2) over one orbit
L3	Geophysical variables averaged in time and mapped on a global longitude/latitude horizontal grid
L4	Model output derived by assimilation of observations, or variables derived from multiple measurements (or both)

Table of Contents

History of modifications 4

List of datasets covered by this document 5

Related documents 5

Acronyms 6

General definitions 9

Table of Contents 10

Scope of the document 12

Executive summary 13

1. Instruments 14

1.1 TANSO-FTS-2 on GOSAT-2 14

2. Input and auxiliary data 15

2.1 Level 1b data of TANSO-FTS-2 onboard GOSAT-2 15

2.2 Other data 16

2.2.1 ECMWF model data 16

2.2.2 SRTM DEM 17

2.2.3 Additional Input Data 17

3. Algorithms 18

3.1 Algorithm overview 18

3.2 Forward Model 19

3.2.1 Model Atmosphere and Optical Properties 20

3.2.2 Modeling the top-of-atmosphere radiances 27

3.3 Inverse algorithm 32

3.3.1 Inversion Procedure 34

3.3.2 Regularization of state vector and iteration strategy 36

3.3.3 Convergence criteria 37

3.4 Cloud Filtering 37

3.5 Scaling of O_2 Cross Sections 38

4. Output data 40

References **41**

Scope of the document

This document is an Algorithm Theoretical Basis Document (ATBD) for the Copernicus Climate Change Service (C3S2, https://climate.copernicus.eu/) greenhouse gas (GHG) component as covered by project C3S2_312a_Lot2.

Within this project satellite-derived atmospheric carbon dioxide (CO_2) and methane (CH_4) Essential Climate Variable (ECV) data products are generated and delivered to ECMWF for inclusion into the Copernicus Climate Data Store (CDS) from which users can access these data products and the corresponding documentation.

The GHG satellite-derived data products are:

- Column-averaged dry-air mixing ratios (mole fractions) of CO_2 and CH_4, denoted XCO_2 (in parts per million, ppm) and XCH_4 (in parts per billion, ppb), respectively.
- Mid/upper tropospheric mixing ratios of CO_2 (in ppm) and CH_4 (in ppb).

This document describes the retrieval algorithms to generate the C3S products CO2_GO2_SRFP and CH4_GO2_SRFP v2.0.0.

These products are XCO_2 and XCH_4 Level 2 products as retrieved from GOSAT-2 using algorithms developed at SRON, The Netherlands.

Executive summary

In this document the retrieval algorithms are described, which are used to generate satellite-derived atmospheric carbon dioxide (CO_2) and methane (CH_4) Climate Data Record (CDR) data products as generated via the C3S2_312a_Lot2 project of the Copernicus Climate Change Service (C3S, https://climate.copernicus.eu/).

This document describes the RemoTeC algorithm for GHG retrieval from the GOSAT-2 instrument. It should be read in conjunction with the MAIN ATBD document, defined in the Related Documents section at the beginning of this document [D1]. The original algorithm is based on the paper of Butz et al., 2009. Tests of the retrieval algorithm have been performed on synthetic GOSAT data (Butz et al., 2010), and real GOSAT data (Butz et al., 2011; Schepers et al., 2012; Guerlet et al., 2012). Here we apply the retrieval to GOSAT-2 data.

The RemoTeC algorithm developed by SRON is a linearised vector radiative transfer model which solves the equation of radiative transfer for back-scattered sunlight. It adopts Philips-Tikonov regularization to apply the inversion, and the Gauss-Seidel method to solve the equation of radiative transfer. The retrieval algorithm aims at inferring an atmospheric state vector from a measurement vector. The state vector is linked to the measurement vector through the true forward model. Among others, the state vector for the full physics model described in this document contains CH_4 and CO_2 sub-columns in 12 vertical layers. These sub-columns are averaged via averaging kernels to obtain the final products, denoted XCH_4 and XCO_2.

The greenhouse gas (GHG) activities of this C3S project and its C3S pre-cursor projects are essentially the operational continuation of the research and development (R&D) pre-cursor projects GHG-CCI and GHG-CCI+ of ESA's Climate Change Initiative (CCI). R&D for the GOSAT-2 products is currently an ongoing activity of the ESA GHG-CCI+ project (see https://climate.esa.int/en/projects/ghgs/).

Section 1 gives an overview of the data product including a description of the GOSAT-2 satellite instrument TANSO-FTS-2. Section 2 introduces the various input data which enter into the retrieval algorithm such as meteorological data, satellite level 1 data and a priori CH_4/CO_2 profiles. Sections 3 and 4 describe in detail the retrieval algorithm and its output, respectively.

1. Instruments

1.1 TANSO-FTS-2 on GOSAT-2

As explained in the Main ATBD (D1), GOSAT-2 is the follow-on satellite to the Greenhouse Gases Observing Satellite (GOSAT) and is thus very similar to its predecessor. The information in D1 provides an overview of GOSAT and GOSAT-2. In this section we provide a more detailed summary of GOSAT-2. We emphasise that the products described in this document are derived only from GOSAT-2.

The Japanese Greenhouse gases Observing SATellite-2 (GOSAT-2) was launched on 29th October 2018 and started operational observations form February 2019. GOSAT-2 provides dedicated global measurements of total column CO_2 and CH_4 from its Short Wave Infra-red (SWIR) bands. It is equipped with two instruments, the Thermal And Near Infrared Sensor for carbon Observations - Fourier Transform Spectrometer-2 (TANSO-FTS-2) as well as a dedicated Cloud and Aerosol Imager-2 (TANSO-CAI-2). For the products described in this document, cloudy scenes are identified via the retrieved columns of oxygen, carbon dioxide and water vapour (section 3.4) thus we do not use data from TANSO-CAI.

The TANSO-FTS-2 instrument (Nakajima et al., 2017) has five spectral bands, illustrated in Table 1, with a high spectral resolution: 0.2 cm^{-1}. Three bands operate in the SWIR at 0.75-0.77, 1.56-1.69 and at the extended 1.92-2.33 µm range, providing sensitivity to the near-surface absorbers. The fourth and fifth channels operating in the thermal infrared between 5.5-8.4 and 8.4-14.3 µm providing mid-tropospheric sensitivity.

FTS-2 observes sunlight reflected from the earth's surface and light emitted from the atmosphere and the surface. The former is observed in the spectral bands 1 through 3 of FTS-2 in the daytime, and the latter is captured in band 4 and 5 during both the day and the night. Within this project only level 1 data from the SWIR channels 1-3 will be used. Prior to reaching the detectors of the instrument, the light in the bands 1 through 3 is split into two orthogonally-polarised components and measured independently. The intensity component of Stokes vector is approximated by the mean of parallel (P) and perpendicular (S) components (O'Brien et al., 2013).

Table 1: TANSO-FTS-2 bands.

Channel	Wavelength range [nm]	Resolution [cm^{-1}]
1	758-775	0.2
2	1460-1720	0.2
3	1920-2330*	0.2
4	5560-8400	0.2
5	8400-14300	0.2

*GOSAT-1 only had a spectral range up to 2080nm.

The measurement strategy of TANSO-FTS-2 is optimised for the characterization of continental-scale sources and sinks. TANSO-FTS-2 utilizes a pointing mirror to perform off-nadir measurements at the same location on each 6-day repeat cycle. The pointing mirror allows TANSO-FTS-2 to observe up to ±35° across track and ±40° along-track. These measurements nominally consist of 5 across track points spaced ~160km apart with a ground footprint diameter of approximately 9.7 km and a 4 second exposure duration. The satellite has an Intelligent pointing Monitor camera which makes it possible to adjust the line of sight of the FTS to steer away from cloud contaminated areas. Whilst the majority of data is limited to measurements over land where the surface reflectance is high, TANSO-FTS-2 also observes in sunglint mode over the ocean. More information on GOSAT-2 can be found here: http://www.gosat-2.nies.go.jp/.

2. Input and auxiliary data

The following section describes the various data that are associated with the full physics retrieval. The input measurement for the forward model consist of the GOSAT-2 L1B TANSO-FTS-2 data (section 2.1) and the other data used is auxiliary data such as ECMWF model data, the SRTM DEM, etc. (section 2.2).

2.1 Level 1b data of TANSO-FTS-2 onboard GOSAT-2

Level 1b data of the TANSO-FTS-2 on-board GOSAT-2 are needed in the project to produce the total column CO_2 and CH_4 products. They serve as input for the retrieval algorithms to be used in this project.

TANSO-FTS-2 level-1b data are available since February 2019. The GOSAT-2 FTS L1A/L1B Product Description Document (Japan Aerospace Exploration Agency, July 2019, GST-18005) is available through https://prdct.gosat-2.nies.go.jp/documents/pdf/NIES_GOSAT-2_Product_File_Format_Descriptions_en_03.pdf

The quality of the retrieved CO_2 and CH_4 columns has been tested against ground-based observations (section 2.2.2) and has shown to be of good quality. The spectral bands showed some irregularities which required a shortened retrieval window (O_2 A-band) and spectral intensity offsets for each of the bands. This in effect worsened the cost function χ^2 of the fits compared to similar GOSAT-1 retrievals and the estimated uncertainties of the species. However, validation with respect to ground-based observations showed that the retrieval products of both the GOSAT-1 and GOSAT-2 are of similar quality.

2.2 Other data

2.2.1 ECMWF model data

The retrieval algorithms to produce vertical columns of CO_2 and CH_4 need as input for each scene the temperature vertical profile, pressure vertical profile, specific humidity vertical profile, and wind speed. Here, temperature and pressure are needed to calculate absorption cross sections, the specific humidity vertical profile is needed to account for water vapor absorption, and the wind speed is needed to calculate the Fresnel reflection contribution on a rough ocean surface. The meteorological data mentioned above will be taken from the ECMWF model.

ECMWF has developed one of the most comprehensive earth-system models available anywhere. The ECMWF model uses the '4D-Var' data assimilation approach, which provides a physically consistent best fit to observations. For this project the ERA-5 data are used. The ECMWF model data sets are widely considered to be among the best available data sets for meteorological parameters. We have compared retrievals for an overlapping month (August 2019) using both ERA-5 and ERA-interim and no major effects were observed in the retrieved parameters. The source and description of the ECMWF data used can be found in Table 2.

Table 2: Summary of ECMWF atmospheric data used for trace gas retrieval.

Model	ECMWF ERA-5 atmospheric model
Type	Reanalysis complete
Stream	oper
class	ea
Availability	01/08/2019 to present
Coverage	Global scale
Spatial grid	0.75x0.75 deg
Time grid	6 hours
Number of levels	137
Parameters (levels)	• temperature, specific humidity (all levels) • logarithm of surface pressure, geopotential (lowest level)
Parameters (surface)	• 10 meter U wind component • 10 meter V wind component

2.2.2 SRTM DEM

The RemoTeC retrieval algorithm for CO_2 and CH_4 columns from GOSAT-2 use information about the surface elevation from an extended SRTM digital elevation map available from (http://www.viewfinderpanoramas.org/dem3.html).

The original Shuttle Radar Telemetry Mission (SRTM) was provided by the United States National Aeronautics and Space Administration (NASA). The dataset used (DEM3) is based on the SRTM dataset and includes extrapolation and gap filling from various sources.

The original SRTM dataset provides elevation data ranging from 56 degrees south to 60 degrees north at a 90 meter resolution. The adjusted DEM3 dataset extends the coverage, while keeping the 90 meter resolution.

2.2.3 Additional Input Data

- Absorption cross sections: For the retrieval lookup-tables are used with pre-calculated absorption cross sections of the species of interest (O_2, CO_2, CH_4, and H_2O) as a function of wavenumber, temperature, and pressure. One lookup-table per species and per spectral band is used. At the start of processing, the cross-section lookup table is read into memory.
- Aerosol optical properties: A lookup table is used with pre-calculated aerosol optical properties (Mie and t-Matrix theory) as a function of size parameter and refractive index.
- Solar source: The solar source for the forward simulation uses data of extraterrestrial irradiance from the Total and Spectral Solar Irradiance Sensor-1 Hybrid Solar Reference Spectrum (TSIS-1 HSRS). It covers a temporally constant irradiance spectrum between 200 and 2700 nm with a spectral resolution of 0.001 nm (Coddington et al., 2021). The TSIS-1 HSRS data is downloaded from https://lasp.colorado.edu/lisird/data/tsis1_hsrs .
- Retrieval settings: A file which contains retrieval settings covering instrument characteristics (like the full width half maximum (FWHM) of the instrument profile), spectral window information and spectral sampling, absorbing molecules and profile inversion methods.

3. Algorithms

In order to account for the effect of aerosols and cirrus, the developed algorithm retrieves the methane column simultaneously with the aerosol/cirrus amount (column integrated particle number concentration), a parameter related to the particle size distribution, and a parameter describing the height distribution. Here, the particle size distribution is described by a power-law function, which only has two free parameters (related to amount and size). The choice of aerosol/cirrus parameters reflects the information content of the measurements as closely as possible. The retrieval algorithm uses measured radiances in the Short Wave Infra-Red (SWIR) band and additionally in the Near Infra-Red (NIR, O_2 A-band). Additional fit parameters are the surface albedo and its 1st order spectral dependence in all bands, and the total column of water vapor, respectively.

In order to obtain a proper characterization of the retrieved XGHG, it is important to first retrieve a vertical profile (layer averaged number density in different layers of the model atmosphere) and use this retrieved vertical profile to calculate the vertical column. Here, we choose to provide the vertical column as a product, and not the full profile, because the Degrees of Freedom for Signal (DFS) of the retrieved CH_4 and CO_2 profile is about 1. The inversion is performed using Phillips-Tikhonov regularization in combination with a reduced step size Gauss-Newton iteration scheme.

The forward model of the retrieval algorithm uses online radiative transfer calculations, fully including multiple scattering. Here, the radiative transfer model developed by Landgraf et al., 2001, and Hasekamp and Landgraf 2002, 2005 is being used. This model uses the Gauss-Seidel iterative method to solve the radiative transfer equation in a plane-parallel, vertically inhomogeneous atmosphere. To avoid time consuming line-by-line calculations we employ the linear-k method developed by Hasekamp and Butz 2008. Absorption cross sections of the relevant atmospheric trace gases are tabulated in a lookup table as function of pressure and temperature. Optical properties of aerosols are also calculated from lookup tables as described in Dubovik et al. 2006. The linear k-binning method in combination with other speed optimizations allow us to perform the GHG retrievals from GOSAT-2 with online RT calculations within ~60 seconds for a single retrieval. This makes the algorithm feasible for global processing.

3.1 Algorithm overview

Any retrieval algorithm aims at inferring an atmospheric state *vector x* from a measurement vector *y*. The state vector is linked to the measurement vector through the true forward model *f(x,b)* that depends on the state *vector x* and the *vector b* containing ancillary parameters that are not retrieved,

$$y = f(x, b) + e_y \quad (1)$$

Where e_y represents the measurement noise vector. A retrieval method approximates the true forward model *f* by a retrieval forward model *F*, with a forward model error vector e_F,

$$\mathrm{y} = \mathrm{F}(x, b) + \mathrm{e}_{\mathrm{y}} + \mathrm{e}_{\mathrm{F}} \quad (2)$$

For full physics retrieval from the TANSO -FTS-2 instrument the measurement vector contains the measured intensities in the NIR and SWIR (see Table 3).

Table 3: Spectral ranges from the NIR and SWIR band included in the measurement vector.

Band	Used spectral range (nm)
1 (O_2 a)	757.863 – 772.201
2 (CO_2)	1593.118 – 1620.746
3 (CH_4)	1629.195 – 1654.260
4 (CO_2)	2042.484 – 2080.732

For the retrieval procedure it is needed that the non-linear forward model is linearised so that the retrieval problem can be solved iteratively. For iteration step *n* the forward model is approximated by

$$\mathrm{F}(\mathrm{x}, \mathrm{b}) \approx \mathrm{F}(\mathrm{x}_n, b) + \mathrm{K}(\mathrm{x}_n - \mathrm{x}) \quad (3)$$

Where x_n is the state vector for the n-th iteration step and *K* is the Jacobian matrix

$$\mathrm{K} = \frac{\partial \mathrm{F}}{\partial \mathrm{x}} \quad (4)$$

Below, we will describe the retrieval forward model, state vector, ancillary parameter vector, and the inversion method in more detail.

3.2 Forward Model

The retrieval forward model *F* simulates the measurement vector *y* for a given model atmosphere defined by the state vector *x* and the ancillary parameter vector *b*. The simulated intensity for a given spectral pixel *i* is given by

$$I_i = \int_{\lambda_{min}}^{\lambda_{max}} I(\lambda) S_i(\lambda) d\lambda \quad (5)$$

Where $S_i(\lambda)$ is the Instrument Spectral Response Function (ISRF) for spectral pixel *I* and $I(\lambda)$ is the modeled intensity at high spectral resolution. In the NIR and SWIR channel $I(\lambda)$ contains many fine

spectral structures due to molecular absorption, so it has to be calculated at fine spectral resolution (0.1 cm^{-1} in the NIR band and 0.02 cm^{-1} in the SWIR).

The different steps of the forward model calculation are summarised in Figure 1.

Figure 1: Overview of forward model.

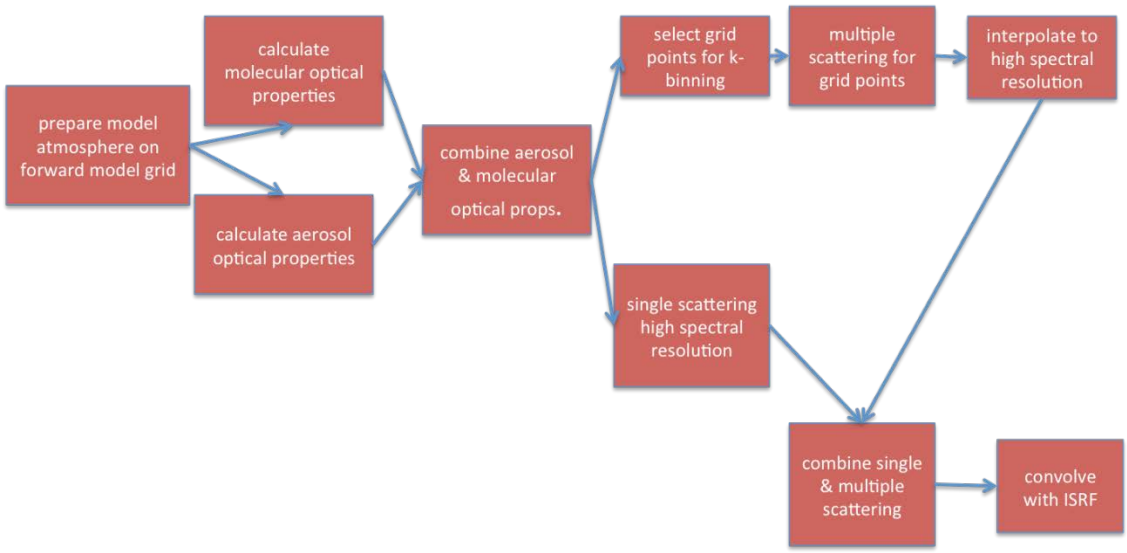

3.2.1 Model Atmosphere and Optical Properties

For the RemoTeC algorithm described here the model atmosphere is defined for *NLAY*=36 homogeneous vertical layers that are equidistant in pressure, the lowest pressure level being defined by the surface pressure. The absorbing trace gases of interest are O_2 (in the NIR band) and CH_4, H_2O, and CO in the SWIR band. The layer sub-columns of these gases are for the first iteration step of each retrieval calculated from the input profiles of CH_4, CO (TM5) and H_2O (ECMWF) and the temperature and pressure profiles (ECMWF). They are obtained on the grid of the model atmosphere by linear interpolation. Here, first the surface pressure p_{surf} is obtained by interpolation of the input pressure profile as function of height to the surface height (input) for the corresponding ground pixel. Next the pressure values at the layer boundaries are calculated, with the pressure p_k at the lower boundary of layer k (counting from top to bottom) is given by:

$$p_{lev,k} = p_{min} + \Delta p * k \quad (6)$$

Where:

$$\Delta p = \frac{p_{surf} - p_{min}}{NLAY} \quad (7)$$

Where p_{min} is the pressure value of the upper boundary of the input (ECMWF) atmosphere. The different atmospheric profiles are constructed on this pressure grid. For example, the methane sub-column DV_CH4_k for the layer bounded by pressure levels $p_{lev,k}$ and $p_{lev,k+1}$ is given by:

$$DV\_CH4_k = XCH4_k \times DV\_AIR_k \quad (8)$$

Where $XCH4_k$ is the methane dry air mixing ratio linearly interpolated from the input pressure grid to the pressure at the 'middle' of layer k defined by $(p_k+p_{k+1})/2$. DV_AIR_k is the sub-column of air in layer *k*, given by

$$DV\_AIR_k = (p_{lev,k+1} - p_{lev,k}) \times R/(M \times g_k \times \left(1 + \frac{XH_2O_k}{1.60855}\right)) \quad (9)$$

Where R is Avogadro's number, M is the molecular mass of air, g_k is the gravity constant in altitude layer k, and 1.60855 is the mass of air relative to the mass of water (Wunch et al., 2010). The sub columns of CO and H_2O are calculated in the same manner as for CH_4, and the O_2 sub-column is obtained by multiplying the air sub-column by the O_2 mixing ratio (=0.2095).

For a radiative transfer calculation at a given wavelength the layer absorption optical thickness, scattering optical thickness, and scattering phase function for each model layer are needed. For layer *k* of the model atmosphere the CH_4 absorption optical thickness at wavelength λ_j is calculated by:

$$\tau_{abs,ch4}(\lambda_j) \sum_{i=1}^{N} \sigma\left(p_i T_i \lambda_j\right) * DV\_CH4_k/N \quad (10)$$

Where N is the number of sub-layers in which the model atmosphere layers are divided (set at N=2) and σ is the absorption cross-section of CH_4 at wavelength λ_j and the pressure p_i and temperature T_i for the middle of model sub-layer i. The absorption optical thickness for the other trace gases is calculated in the same way. Pre-calculated absorption cross-sections for CH_4, CO, H_2O, and O_2 are stored as lookup-table as a function of pressure, temperature, and wavenumber. These cross-section lookup-tables are calculated from the latest spectroscopic databases (Jenouvrier et al., 2007; Rothman et al., 2009) assuming Voigt line shapes. For water vapor, an updated spectroscopic line list has been developed by Scheepmaker et al. 2012. In the NIR spectral range the absorption cross sections of O_2 are calculated according to Tran et al. 2006 taking into account line mixing and collision induced absorption. The cross-section for pressure p_i, temperature T_i and wavelength λ_j are obtained by linear interpolation from the tabulated values. The reason that each of the NLAY layers of the model atmosphere is further divided into N sub-layers, is to properly account for the strong dependence of temperature and pressure of the absorption cross-sections. So, the absorption cross-sections are needed for NLAY X N = 36 X 2=72 vertical layers equidistant in pressure.

The total molecular absorption optical thickness is obtained by summing the contribution of the different trace gases. The Rayleigh scattering optical thickness for layer k and wavelength λ_j is given by

$$\tau_{ray,k}(\lambda)_j = \sigma_{ray}(\lambda)_j * DV\_AIR_k \quad (11)$$

Where σ_{ray} is the Rayleigh scattering cross section given by (*Buchholtz,1995*)

$$\sigma_{ray}(\lambda) = A\,\lambda^{-(4+X)} \quad (12)$$

Where:

$$X = B\lambda + \frac{C}{\lambda} - D \quad (13)$$

With *A*= 4.02E-28, *B*=0.389, *C*=0.04926, *D*=0.3228.

The Rayleigh scattering phase function is given by (e.g. Hansen and Travis, 1974)

$$P(\Theta) = \frac{3}{4}(1 + cos^2\Theta)\frac{(1-\delta)}{(1+\frac{\delta}{2})} \quad (14)$$

Where δ is the depolarization ratio and Θ is the scattering angle defined by

$$\cos(\Theta) = -u_0 u_v + \sqrt{(1-u_v)^2}\sqrt{(1-u_{v0})^2}\cos(\varphi_0 - \varphi_v) \quad (15)$$

Where u_0 and u_v are the cosines of the solar and viewing zenith angle, respectively (absolute values) and φ_0 and φ_v are the solar and viewing azimuth angles.

In addition to trace gases, also aerosols are present in the model atmosphere. In our algorithm, aerosols are described by the following parameters (following Butz et al. (2009;2010)):

1. Number of particles in each layer of the model atmosphere. This is provided by the total amount of particles, N_{aer}, and a normalised altitude distribution described by a Gaussian function of center height z_{aer} and width w_0. Hence, in model layer k with central height z_k, the number of particles is given by $h(z_k) = N_{aer}\exp\left[-\frac{4\ln(z_k - z_{aer})^2}{(2w_0)^2}\right]$

2. A size distribution of $n_{aer}(r)$, described by a power law size function, characterised by power law exponent and upper and lower cut-off (e.g. Mishchenko et al., 1999).

$$n(r) = \begin{cases} A & r \leq r_1 \\ A(r/r_1)^{-\alpha} & r_1 < r \leq r_2 \\ 0 & r > r_2 \end{cases} \quad (16)$$

The cut-offs are r_1,=0.1μm, r_2 = 10 μm and the constant A is determined from normalization of the size distribution. Figure 2 illustrates $n_{aer}(r)$ and compares it to a more realistic multimodal lognormal size distribution (Stier et al., 2005). Through its parameter α, the aerosol size distribution controls the spectral dependence of aerosol optical properties among the considered retrieval windows.

3. The complex refractive index m =m_r+im_i, which is assumed independent of wavelength within a retrieval window.

Figure 2: Aerosol size distribution $n_{aer}(r)$ as a function of particle radius r. The retrieval method relies on a power law (red solid) size distribution. Also shown are more realistic Multi-modal lognormal size distributions for a fine mode (black dashed) and a coarse mode (black dotted) dominated aerosol type.

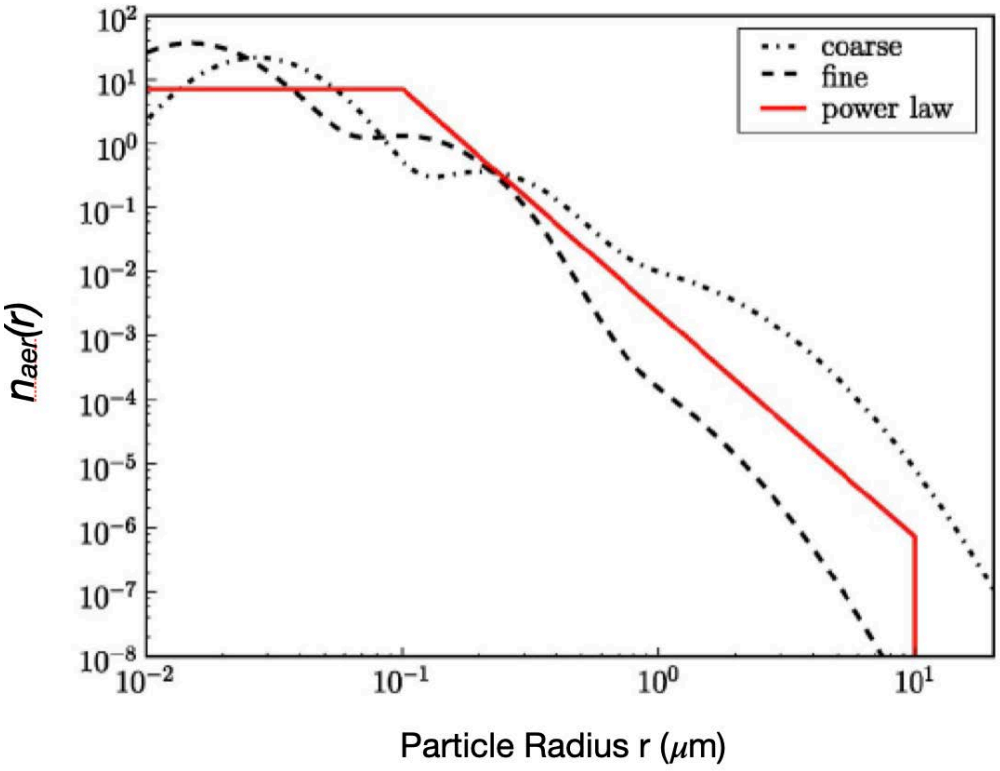

From the aerosol size distribution, refractive index, and number of particles of each layer the aerosol scattering optical thickness $\tau_{scat,aer}$ and aerosol absorption optical thickness $\tau_{abs,aer}$ are calculated

$$\tau_{scat,aer}(z_k) = \sigma_{scat,aer} h(z_k) \quad (17)$$

and

$$\tau_{abs,aer}(z_k) = \sigma_{abs,aer} h(z_k) \quad (18)$$

Where $\sigma_{scat,aer}$ and $\sigma_{abs,aer}$ are the aerosol scattering and absorption cross-section, respectively. They are obtained by:

$$\sigma_{scat,aer} = \sum_{i=1}^{M} K_{scat,i}(m) r_i n_{aer}(r_i) v(r_i) \quad (19)$$

Where:

$$K_{scat,i} = \int_{\Delta ln r_i} \frac{\sigma_{scat}(r,m)}{v(r)} d \ln r \quad (20)$$

Where v denotes particle volume and $K_{scat,i}$,representative for particle radius r_i, is pre-calculated for M size bins according to Dubovik et al., 2006 and stored in a lookup table as function of aerosol size parameter $x=2\pi r/\lambda$, real refractive index, and imaginary refractive index. The values for the actual aerosol refractive index are obtained by linear interpolation from the tabulated values. The lookup table contains values for spheres (Mie calculations) as well as for spheroids with a pre-defined axis ratio distribution (Dubovik et al, 2006) but in our algorithm baseline we only consider spherical particles. Similar expressions hold for the absorption cross-section and the aerosol scattering phase function.

Finally, the total optical properties per layer in the model atmosphere are obtained by combining the contribution of gases and aerosols:

$$P(\Theta) = \frac{\tau_{sca,mol} P_{mol}(\Theta) + \tau_{sca,aer} P_{aer}(\Theta)}{\tau_{sca,mol} + \tau_{sca,aer}} \quad (21)$$

Where:

$$\tau_{abs} = \tau_{abs,mol} + \tau_{abs,aer} \quad (22)$$

And

$$\tau_{sca} = \tau_{sca,mol} + \tau_{sca,aer} \quad (23)$$

For multiple scattering calculations the scattering phase function is needed in the form of expansion coefficients for generalised spherical functions, where expansion coefficient α_l with index *l* is given by:

$$\alpha^l = \frac{2l+1}{2}\int_{-1}^{1} P_{0,0}^l(cos\Theta)P(\Theta)dcos\Theta \quad (24)$$

Where $P_{0,0}^l$ is element (1,1) of the Generalised Spherical Function matrix (e.g. de Haan et al., 1987).

To summarize, the forward model needs the following inputs:

- Surface pressure to define the equidistant pressure grid
- Sub-columns of CH_4, CO, H_2O, O_2, and air for the vertical layers of the model atmosphere.
- Pressure and temperature at the middle of the model sub-layers for absorption cross-sections.
- The aerosol column N_{aer}.
- The aerosol size parameter α (power of the power law size distribution function).
- The central height z_{aer} and width w_0 of the Gaussian aerosol altitude distribution.
- Solar Zenith Angle (SZA).
- Viewing Zenith Angle (VZA).
- Relative Azimuth Angle (RAA).
- The aerosol complex refractive index $m = m_r + im_i$
- A high spectral resolution solar reference spectrum.
- Lookup tables with absorption cross-sections of CH_4, CO, H_2O, and O_2 as function of pressure, temperature, and wavenumber.
- Lookup tables with pre-calculated aerosol properties as function of aerosol size parameter, real refractive index, and imaginary refractive index (cross sections and phase functions integrated over each size parameter bin).

Based on these inputs the optical properties can be calculated for each layer of the model atmosphere.

3.2.2 Modeling the top-of-atmosphere radiances

Based on the optical properties (τ_{abs}, τ_{sca}, $P(\Theta)$) defined for each wavelength and layer of the model atmosphere we can compute the top-of-atmosphere radiance as measured by the instrument. The first step is to separate the radiation field in a singly scattered component $\boldsymbol{I}_{ss}$ and a multiply scattered component $\boldsymbol{I}_{ms}$, respectively:

$$I = I_{ss} + I_{ms} \tag{25}$$

The computation of I_{ss} for a given wavelength is straightforward:

$$\begin{aligned} I_{ss} = F_0 \sum_{k=1}^{NLAY} \omega_k P_k(\Theta) \left[1 - e^{-(\tau_{tot,k}\left(\frac{1}{u_0}+\frac{1}{u_v}\right)}\right] u_0 \\ /4\pi(u_o + u_v) e^{-(\sum_{i=1}^{k} \tau_{tot,i}/u_0)} e^{-(\sum_{i=1}^{k} \tau_{tot,i}/u_v)} \\ + e^{-(\sum_{k=1}^{NLAY} \tau_{tot,i}/u_0)} e^{-(\sum_{k=1}^{NLAY} \tau_{tot,i}/u_{0v})} R_{surf} \end{aligned} \tag{26}$$

Where F_0 is the incoming total flux, $\tau_{tot} = \tau_{abs} + \tau_{sca}$, $\omega = \tau_{sca}/\tau_{tot}$, u_0 is the cosine of the solar zenith angle, u_v is the cosine of the viewing zenith angle, and R_{surf} is the surface reflection for the specific solar and viewing geometry under consideration. Besides the I_{ss} itself, also the derivatives with respect to $\tau_{sca,k}$, $\tau_{abs,k}$ ω_k and P_k are needed:

$$\begin{aligned} \frac{\partial I_{ss}}{\partial \tau_{tot,k}} = F_0 \omega_k P_k(\Theta) \left[e^{-(\tau_{tot,k}\left(\frac{1}{u_0}+\frac{1}{u_v}\right)}\right] u_0 / 4\pi(u_o + u_v) e^{-(\sum_{i=1}^{k} \tau_{tot,i}/u_0)} e^{-(\sum_{i=1}^{k} \tau_{tot,i}/u_v)} \\ - \sum_{i=1}^{K} \omega_k P_k(\Theta) \left[1 - e^{-(\tau_{tot,k}\left(\frac{1}{u_0}+\frac{1}{u_v}\right)}\right] u_0 \\ /4\pi(u_o + u_v) e^{-(\sum_{i=1}^{k} \tau_{tot,i}/u_0)} e^{-(\sum_{i=1}^{k} \tau_{tot,i}/u_v)} \end{aligned} \tag{27}$$

$$\frac{\partial I_{ss}}{\partial P_k} = F_0 u_0 / 4\pi(u_o + u_v) e^{-(\sum_{i=1}^{k} \tau_{tot,i}/u_0)} e^{-(\sum_{i=1}^{k} \tau_{tot,i}/u_v)} \left[1 - e^{-(\tau_{tot,k}\left(\frac{1}{u_0}+\frac{1}{u_v}\right))}\right] \omega_k \quad (28)$$

$$\frac{\partial I_{ss}}{\partial \omega_k} = F_0 u_0 / 4\pi(u_o + u_v) e^{-(\sum_{i=1}^{k} \tau_{tot,i}/u_0)} e^{-(\sum_{i=1}^{k} \tau_{tot,i}/u_v)} P_k(\Theta) \left[e^{-(\tau_{tot,k}\left(\frac{1}{u_0}+\frac{1}{u_v}\right))}\right] \quad (29)$$

$$\frac{\partial I_{ss}}{\partial \tau_{sca,k}} = \frac{\partial I_{ss}}{\partial \omega_k} \frac{1}{\omega_k} - \frac{\partial I_{ss}}{\partial \tau_{tot,k}} \quad (30)$$

$$\frac{\partial I_{ss}}{\partial \tau_{abs,k}} = \frac{\partial I_{ss}}{\partial \tau_{tot,k}} - \frac{\partial I_{ss}}{\partial \omega_k} \omega_k / \tau_{tot,k} \quad (31)$$

The computation of the multiply scattered radiation for a given wavelength involves the solution of the plane-parallel radiative transfer equation. We solve this equation using the Gauss-Seidel iterative method. The solution is described in detail by Landgraf et al., 2001 and will not be repeated here. The calculation of the derivatives with respect to optical properties per layer k of the model atmosphere is performed using the forward adjoint perturbation theory and is described in detail by Hasekamp and Landgraf (2005a).

The radiative transfer calculations yield the derivatives of the radiance with respect to the optical parameters τ_{sca}, τ_{abs}, and P or its expansion coefficients α_l. From these derivatives, the derivatives with respect to a physical parameter x can be calculated in a straightforward manner by the derivative chain rule

$$\frac{\partial I_{ss}}{\partial x} = \sum_{k=1}^{NLAY} \frac{\partial I_{ss}}{\partial \tau_{sca,k}} \frac{\partial \tau_{sca,k}}{\partial x} + \frac{\partial I_{ss}}{\partial \tau_{abs,k}} \frac{\partial \tau_{abs,k}}{\partial x} + \frac{\partial I_{ss}}{\partial P_k} \frac{\partial P_k}{\partial x} \tag{32}$$

$$\frac{\partial I_{ms}}{\partial x} = \sum_{k=1}^{NLAY} \frac{\partial I_{ms}}{\partial \tau_{sca,k}} \frac{\partial \tau_{sca,k}}{\partial x} + \frac{\partial I_{ms}}{\partial \tau_{abs,k}} \frac{\partial \tau_{abs,k}}{\partial x} + \sum_{l=0}^{M} \frac{\partial I_{ms}}{\partial \alpha_k^l} \frac{\partial \alpha_k^l}{\partial x} \tag{33}$$

In order to avoid time consuming multiple scattering calculations on the high spectral resolution line-by-line grid we aim at reducing the number of spectral calculations, following the approach of Hasekamp and Butz 2008. For this purpose, we consider the intensity $\boldsymbol{I}_{ms}$ as a function of total absorption optical thickness τ_{abs} and its normalised vertical distribution n (similar to k-distribution and spectral mapping methods),

$$I_{ms}(\lambda) = I_{ms}(\tau_{abs}(\lambda), \boldsymbol{n}(\lambda)) \tag{34}$$

Where we assume that the atmospheric scattering properties and surface reflection properties are constant over the spectral range under consideration. Here, the explicit separation between total absorption optical thickness and its vertical distribution is chosen for later convenience. Element n_k of the vector n represents the relative contribution of the absorption optical thickness of altitude layer k of the model atmosphere to the total absorption optical thickness of the atmosphere, such that

$$\tau_{abs}^k(\lambda) = n_k(\lambda)\tau_{abs}(\lambda) \tag{35}$$

Where τ^k_{abs} is the absorption optical thickness of layer k of the model atmosphere.
For a vertically homogeneous atmosphere the advantage of the description as function of absorption optical thickness is obvious. Namely, the intensity depends smoothly on absorption optical thickness, which means that only calculations at a limited number of values of τ_{abs} are needed from which the Stokes parameters at other values of τ_{abs} can be obtained by interpolation (see e.g. van Diedenhoven et al., 2006). Finally, the Stokes parameters can be mapped back into wavelength space. To apply this procedure for a non-homogeneous atmosphere, one has to

assume that the vertical distribution *n(z)* of τ_{abs} can be approximated by a vertical distribution that is independent of wavelength in the spectral interval under consideration. This is the underlying assumption of the correlated k method. For the simulation of moderate- or high resolution spectra in the near- and shortwave infrared spectral ranges, this assumption may cause errors of several percent in reflectance spectra for realistic inhomogeneous terrestrial atmospheres (see e.g. Duan et al., 2005).

Clearly, an efficient radiative transfer model is needed that accounts for the vertical distribution of absorption optical thickness at different wavelengths. For this purpose we use the transformation into absorption optical thickness space, and perform calculations for a limited number *N* values of τ^k_{abs} of the absorption optical thickness and corresponding vertical distributions n^k, with k=1,…,N. From the reference calculations $I_{ms}(\tau^k_{abs}, n^k)$ we want to obtain the multiply scattered intensity vector $I_{ms}(\lambda_j)$ at any wavelength λ_j in the spectral range under consideration with absorption optical thickness $\tau_{abs}(\lambda_j)$ and its vertical distribution $n(\lambda_j)$.

The basic principle of our linear-k method is to account for differences between the actual vertical distribution $n(\lambda_j)$ and the vertical distributions n^k used in the reference calculations, by employing the linear approximation:

$$I_{ms}\left(\tau^k_{abs}, n(\lambda_j)\right) \approx I_{ms}(\tau^k_{abs}, \mathrm{n}^k) + \frac{\partial I_{ms}}{\partial n}\left[n(\lambda_j) - \mathrm{n}^k\right], \tag{36}$$

Where the derivatives with respect to *n* follow from the forward adjoint perturbation theory (Hasekamp and Landgraf, 2005). Applying equation 36 yields the intensity vector of the multiply scattered radiation at the grid points τ^k_{abs}, corrected for the actual vertical distribution. In order to obtain the intensity I_{ms} at $\tau_{abs}(\lambda_j)$ we fit a second order polynomial to the logarithm of the (absorption profile corrected) intensities at the grid points, using the grid points closest to $\tau_{abs}(\lambda_j)$ and the two neighbouring points. In order to correct for variation of scattering properties and surface albedo within the spectral range under consideration, also a linear correction is used.

The grid points are chosen equidistant on a logarithmic scale. For grid point *k* the total absorption optical thickness is given by:

$$\tau^k_{grid} = e^{\log(\tau_{\min})+(k-1)[[\log(\tau_{\max})-\log(\tau_{\min})]/N]} \tag{37}$$

Where τ_{min} and τ_{max} are respectively the minimum and maximum absorption optical thickness in the spectral window under consideration. If τ_{max} is larger than 15 its value is set to 15, because for larger values of the absorption optical thickness the radiation field is dominated by single scattering (being calculated exactly) and hence interpolation errors are of minor importance. The rationale of choosing a logarithmic scale is to obtain more grid points at small values of absorption optical thickness, where multiple scattering effects are most important. If a certain spectral range is influenced by considerable absorption by two or more species we use 2 grids: one for the target absorber and one for the total of other absorbers. For the radiative transfer calculations in the

methane retrieval algorithm we use 10 grid points in the NIR band and 5 X 4 = 20 grid points (5 for CH_4 and 4 for H_2O and CO combined) in the SWIR band. Figure 3 illustrates the accuracy of the linear-k method for the NIR spectral range. For more information on the linear-k method we refer to the paper of Hasekamp and Butz 2008.

Figure 3: Relative difference between a spectrum calculated using the linear-k method and a spectrum obtained using line-by-line calculations. Upper panel shows the intensity and the lower panel the degree of linear polarization. The solid and dashed lines correspond to spectral resolutions of S5P, GOSAT and GOSAT-2, respectively. For the calculations a boundary layer aerosol was used with an optical thickness of 0.3 at 765 nm. Furthermore, we used a solar zenith angle (SZA) of 50° and a viewing zenith angle of 0°.

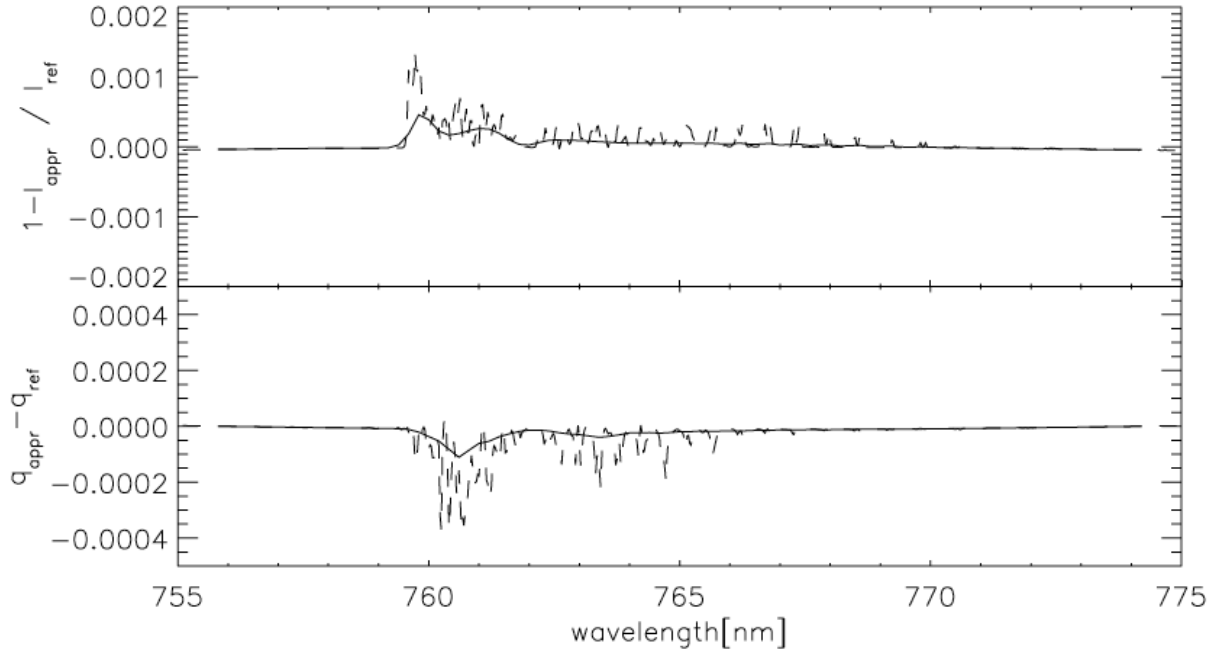

3.3 Inverse algorithm

Definition of state vector and ancillary parameters

The **state vector x** contains the following elements (between brackets are optional elements):

- CO_2 sub-columns in 12 vertical layers (layer interfaces coincide with *NLAY* layers of forward model grid).
- CH_4 sub-columns in 12 vertical layers (layer interfaces coincide with *NLAY* layers of forward model grid).
- H_2O total column.
- Aerosol parameter N_{aer} (number column).
- Aerosol parameter α (size parameter).
- Aerosol parameter z_{aer} (central height of Gaussian height distribution).
- Lambertian surface albedo in all bands band.
- First order spectral dependence of surface albedo in all bands.
- Spectral shift of Earth radiances in all bands (higher orders optional).
- Spectral shift of Earth radiances in all bands (higher orders optional).
- Intensity offset in the NIR band.
- (Offset in input temperature profile).
- (Surface pressure).

For convergence it was essential to include intensity offsets for each of the individual spectral windows. Potentially there are still irregularities in the quality of the individual spectral bands. Table 4 summarises the sources of several key a priori information.

The **ancillary parameter vector b** contains the following parameters:

- H_2O sub-columns in 36 vertical layers of forward model grid.
- Temperature vertical profile at 72 layers of cross-section vertical grid.
- Pressure vertical profile at 72 layers of cross-section vertical grid.
- The aerosol complex refractive index (fixed at 1.4-0.01i for NIR and 1.47-0.008i for SWIR).
- The width w_o of the Gaussian aerosol height distribution (fixed at 2000 meter).

Table 4: A priori values for the different state vector elements.

State vector element	A priori value
CH_4 sub-columns	TM4
CO_2 sub-columns	Carbontracker
H_2O total column	ECMWF
N_{aer}	AOT=0.1 @760 nm
α	fixed at 3.5
z_{aer}	fixed at 5000 meter
surface albedo (NIR + SWIR)	no prior value needed (first guess at maximum of measured reflectance)
spectral shifts	no prior needed (first guess = 0)
temperature offset	no prior needed (first guess = 0)
surface pressure	ECMWF + SRTM DEM

3.3.1 Inversion Procedure

The inverse method optimizes the state vector *x* with respect to the measurements *y* after applying the forward model *F* to *x*. The inverse method is based by default on a Phillips-Tikhonov regularization scheme (Phillips, 1962; Tikhonov, 1963; Hasekamp and Landgraf, 2005a). Regularization is required because the inverse problem is ill-posed, i.e., the measurements *y* typically contain insufficient information to retrieve all state vector elements independently. The inverse algorithm finds *x* by minimizing the cost function that is the sum of the least-squares cost function and a side constraint weighted by the regularization parameter γ according to

$$\hat{x} = \min_{x}(||\mathrm{S}_{y}^{-\frac{1}{2}}(\mathrm{F(x)} - \mathrm{y})||^2 + \gamma||\mathrm{W}(\mathrm{x} - \mathrm{x}_a)||^2) \quad (38)$$

Where S_y is the diagonal measurement error covariance matrix, which contains the noise estimate. x_a is an a priori state vector (see Table 4), and *W* is a weighting matrix (see below).

For the linearised forward model for iteration step n, the equation for the updated state vector x_{n+1} reduces to

$$x_{n+1} = \min\left(||K'(x' - x'_n - y'||^2 + \gamma||x' - x'_n||^2\right) \quad (39)$$

With the weighted quantities

$$\mathrm{x'}=\mathrm{Wx},\ \mathrm{y'}=S_y^{-\frac{1}{2}}(y - F(x_n)) \quad (40)$$

and

$$\mathrm{K'} = S_y^{-1/2}KW^{-1} \quad (41)$$

With *K* the Jacobian. The solution reads

$$x_{n+1} = G'y' + A'x'_n + (I - A')x'_{apr} \quad (42)$$

With A' the averaging kernel matrix and G' the contribution function matrix given by

$$A'=G'K' \quad (43)$$

and

$$G'=(K'^{T}K'+\gamma I)^{-1}K'^{T} \quad (44)$$

If the retrieval converges after a given number of steps N (typically 7-8), the final state vector $x_{retr} = x_N$ is related to the true state vector and to the prior via

$$x_{retr} = Ax_{true} + (I - A)x_n + Ge_y + Ge_F \quad (45)$$

The covariance matrix S_x describing the retrieval noise (Ge_y) is given by

$$S_x = GS_yG^T \quad (46)$$

The target retrieval quantity is the column averaged dry air greenhouse gas mixing ratio, XGHG, where GHG denotes either CO_2 or CH_4. This quantity is obtained from the CH_4 and CO_2 entries of the retrieved state vector through

$$XGHG = h^T x_{retr}/V_{air,dry} \quad (47)$$

Where h is the total column operator for methane (summing up the partial columns in the state vector) and $V_{air,dry}$ is the dry air column calculated from the surface pressure and water vapor profile, both obtained from a meteorological model (required as input). The retrieval noise ΔXCH_4 on XCH_4 is given by

$$\Delta XCH_4 = \frac{\sum_{i=1}^{12}\sum_{j=1}^{12} S_{x,i,j}}{V_{air,dry}} \quad (48)$$

And a similar expression for CO_2.

For validation and application purposes it is important to realize that the retrieved XCH_4 or XCO_2 is in fact a representation of $ax_{true}/V_{air,dry}$, where the quantity

$$a = h^T A \quad (49)$$

Is referred to as the column averaging kernel (Rodgers and Connor, 2003).

3.3.2 Regularization of state vector and iteration strategy

To retrieve a meaningful state vector *x*, the side-constraint in the minimization equation should be chosen in a way that contributions from measurement noise are minimised while retaining all valuable information in the first part of the merit-function. The inverse algorithm relies on a regularised Phillips-Tikhonov scheme. The diagonal weighting matrix *W* is given by

$$\mathrm{W} = \mathrm{LW}' \tag{41}$$

With

$$\mathrm{L} = \begin{pmatrix} 1 & -1 & \cdots & & & & \\ -1 & 2 & -1 & & & & \\ \vdots & & \ddots & & \vdots & & \\ & & -1 & 1 & & & \\ & & \cdots & & 1 & & \\ & & & & & \ddots & \\ & & & & & & 1 \end{pmatrix} \tag{42}$$

The upper left 12 by 12 sub matrix works on the state vector elements that contain the CH_4 sub-columns in the 12 altitude layers of the retrieval vertical grid. This sub-matrix corresponds to the matrix product

$$\mathrm{L}_1^T \mathrm{L}_1 \tag{43}$$

Where L_1 is the first derivative matrix. The W'_{jj} is given by 1/MAX[K(1:12,1:12)] for the state vector elements corresponding to the 12 sub-columns of methane,1/MAX[K(:,j)] for the aerosol parameters, and 0 for all other parameters (which means they are not constrained by the side constraint and are retrieved in a least-squares sense). The value for γ is fixed such that the Degrees of Freedom for Signal (DFS) for the methane profile is in the range 1.0-1.5. This value is found empirically.

If the true solution is far from the current iteration x_n and the forward model $F(x_n)$ far from being linear, the linear approximation may fail and yield a solution x_{n+1} that is further away from the true solution than x_n. To avoid diverging retrievals, we use a Gauss-Newton scheme (see for instance *Rodgers 2000*) with reduced step-size by introducing a filter factor that limits the update per iteration step of the state vector. The updated state vector is then given by:

$$x_{n+1} = \Lambda G' y' + A'^{x'_n} + (I - A')x'_{apr} \tag{44}$$

With the filter factor Λ given by

$$\Lambda = \frac{1}{1+\xi}, \xi > 0 \tag{45}$$

If ξ is large the update of the state vector is small. If $\xi = 0$, the equation for the updated state vector (Eqn. 44) is equivalent to the pure Phillips-Tikhonov equation. The iteration is started with a large ξ, typically on the order of 10. It is then reduced or increased in the following iteration steps according to an empirically found scheme similar to Levenberg-Marquardt strategies (*Rodgers, 2000*). We accept solution x'_{n+1} and decrease ξ by a factor of 2.5 if the least squares norm of iteration n+1 is smaller than 1.1 times the least squares norm of iteration n. Otherwise, we discard the solution of iteration n+1, increase ξ by a factor of 2.5 and solve again for x'_{n+1}. If ξ is smaller than a threshold value of 0.05, it is set to zero and the iteration is continued without a reduction in step size, assuming that the current state vector is sufficiently close to the true solution to finally converge.

3.3.3 Convergence criteria

The iteration is terminated and the retrieval is considered to have converged to a valid solution x_{retr} if the following four conditions are all met:

1. The update of the state vector has become smaller than its theoretical uncertainty.
2. The state vector corresponding to CO_2 and/or CH_4 entries have never reached unrealistic values during the retrieval (negative methane densities for instance).
3. The merit-function has not increased for the current iteration step, and the step-size factor has reached 0.
4. The merit-function divided by the degrees of freedom is smaller than 2.0.

3.4 Cloud Filtering

Cloud filtering in RemoTeC is based on retrieved columns of oxygen (VO2), carbon dioxide (VCO2) and water vapor (VH2O) retrieved independently from the 0.75 micron, 1.6 micron, and 2.0 micron bands, respectively, under the assumption of a non-scattering atmosphere: 0.95<VO2_retrieved/VO2_ecmwf<1.02, 0.99<VCO2_1.6micron/VCO2_2.0micron<1.01, 0.95<VH2O_1.6micron / VH2O_2.0micron < 1.07. The rationale for these cloud filters is that scenes with a large light path deviation with respect to a non-scattering atmosphere will result in different CO_2 and H_2O columns retrieved (without scattering) from the 1.6 and 2.0 micron band due to different light path sensitivities in the two bands. Also, the retrieved O_2 column will deviate more from the ECMWF O_2 column for large light path differences with a non-scattering atmosphere. In addition to these filters based on non-scattering retrievals we also filter out cases for which the aerosol filter $f = AOT_{SWIR} \times \frac{h}{\alpha} < 110$. This filters out scenes with high AOT, large particles, high in

the atmosphere, which are the most difficult cases in terms of light path adjustment. In this way we filter out difficult aerosol cases and scenes contaminated with thin cirrus.

3.5 Scaling of O_2 Cross Sections

Butz et al., (2011) proposed a method to discriminate between errors related to unaccounted light scattering effects and other sources of error using ocean-glint observations. The method has been demonstrated using measurements of the TANSO-FTS onboard GOSAT. Figure 4 (adapted from Butz et al., 2013) motivates the general concept by comparing the total column concentration of molecular oxygen ([O_2]) retrieved from TANSO-FTS O_2 A-band (~ 13,100 cm−1) spectra to [O_2] calculated with high accuracy from meteorological support data. The retrievals neglect any (particulate as well as molecular) light scattering effects and, thus, deviations between meteorological and retrieved [O_2] are to be expected. Figure 4 however, shows that these deviations exhibit a quite different pattern for land-nadir and ocean-glint observations. For land nadir, the distribution scatters rather symmetrically about the occurrence peak with a long tail to strong overestimation as well as underestimation. For ocean glint, in contrast, the distribution exhibits a sharp “upper edge” and wide lower tail. The occurrence peak for ocean glint is offset to lower retrieved [O_2] with respect to the land-nadir retrievals. The rationale to explain the observed pattern assumes that, for ocean glint, virtually all scattering effects result in a shortening of the light path while, for land nadir, scattering effects can have a light path enhancing as well as a light path shortening effect. Light path enhancement typically requires a scattering event at the Earth’s surface, which, however, is dark for the off-glint ocean. Retrievals of [O_2] from ocean glint observations therefore virtually always suffer from unaccounted net light path shortening and, thus, yield an underestimation of the true [O_2] if the retrieval algorithm neglects light scattering effects. For land nadir, the trade-off between light path shortening and light path enhancement is largely controlled by surface albedo, which typically varies substantially for land surfaces. This rationale fits the pattern observed in Figure 4., explaining the sharp upper edge and wide lower tail for ocean glint as well as the rather symmetric distribution for land nadir.

If this argument is true, simple “non-scattering” [O_2] retrievals from the O_2 A-band can be used to find an ensemble of clean ocean-glint scenes where light path modification due to scattering effects is negligible. Following our rationale above, the upper edge of ocean-glint retrievals, i.e. the retrievals which show the least underestimation of the expected meteorological O_2 concentration, are the scenes with the least contamination by scattering effects. For the upper edge ensemble, light scattering as a source of error is negligible, making it a good candidate ensemble to examine other sources of error such as spectroscopic uncertainties or instrumental deficiencies. Using this method, we found the need to scale the O_2 absorption cross sections by a factor 1.03 in order to find agreement with the O_2 column inferred from ECMWF data.

Figure 4: Histogram of the ratio between the total column O_2 concentration retrieved from TANSO-FTS O_2 A-band spectra ($[O_2]$) and the expected meteorological O_2 total column concentration ($[O_2, meteo]$). Histograms are shown separately for retrievals from nadir soundings over land (green lines, black fill) and from glint spot soundings over the ocean (red lines, grey fill). The horizontal lines depict the 99th and 95th percentiles and the occurrence peak (from top to bottom). Retrievals neglect molecular as well as particulate light scattering effects and cover more than 3 years of GOSAT operations from June 2009 to September 2012 (1 million nadir soundings, 0.3 million glint soundings). Basic quality screening is based on convergence of the iterative algorithm, instrument anomaly flagging, goodness of fit, and cirrus contamination detectable at the 5160 cm^{-1} water vapor absorption band.

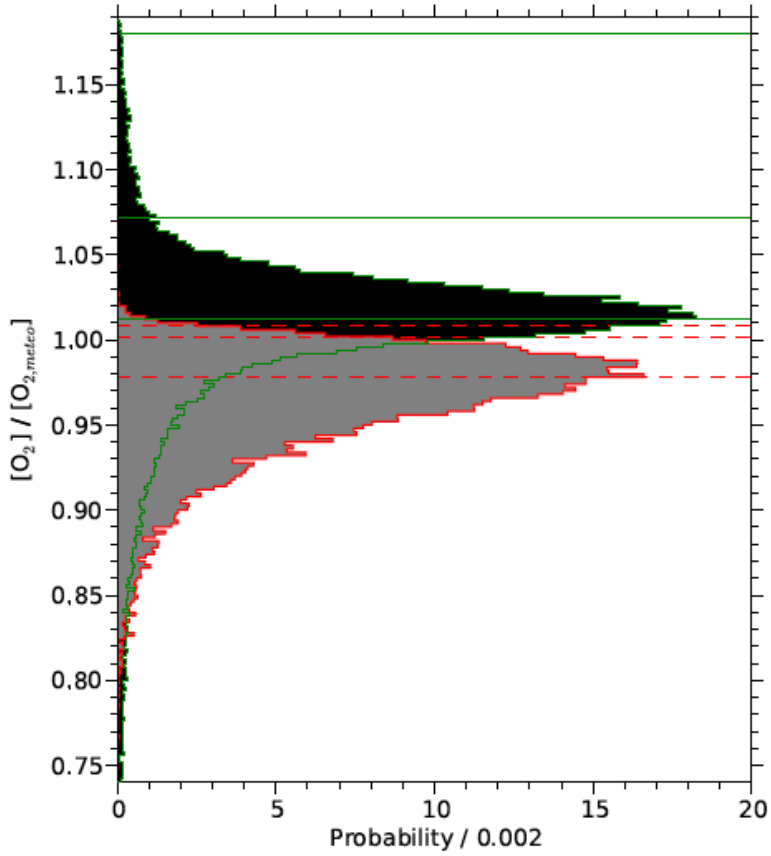

4. Output data

The output data are stored in one NetCDF file per day. The file size varies between 1 and 5 Mb. Separate output files are generated for the XCH_4 Full Physics and the XCO_2 Full Physics products.

The files are named as follows:

ESACCI-GHG-L2-CH4-GOSAT2-SRFP-YYYYMMDD-fv1.nc

Where YYYY, MM and DD denote the year, month and day respectively. The formatting of the files is in accordance with CF-1.6 convention standards and the variable names correspond to CF Standard Name Table v79. There are quality flags "xco2_quality_flag" and “xch4_quality_flag” included in the data files. The quality flag can have 2 values:

- 0: retrieval quality has been checked
- 1: data should not be used (e.g. bad fit to data, residual cloud contamination)

Pixels flagged with 1 include those pixels rejected by post-processing quality filtering steps. After the retrieval step the data that fulfill the following criteria are flagged as '0' for land and ‘1’ for ocean (glint).

An important step in the post-processing is the bias correction (see the Product User Guide and Specification (PUGS) [D2] for details). As a result, two variables are provided for CH_4, defined as xch4 and raw_xch4 for the bias corrected and non-bias corrected columns, respectively. This is also the case for CO_2, with xco2 and raw_xco2 for the bias corrected and non-bias corrected columns, respectively.

Note that the format of the main output data, which are the Level 2 data products, is described in the associated Product User Guide and Specification (PUGS) document [D2] .

References

Buchholtz, 1995: Buchholtz, A. (1995). Rayleigh-scattering calculations for the terrestrial atmosphere. Appl. Opt., 15, 2765

Butz et al., 2009: Butz, A., Hasekamp, O. P., Frankenberg, C., Aben, I. (2009). Retrievals of atmospheric CO2 from simulated space-borne measurements of backscattered near-infrared sunlight: Accounting for aerosol effects. Appl. Opt., 48, 3322.

Butz et al., 2010: Butz, A., Hasekamp, O. P., Frankenberg, C., Vidot, J., and Aben, I.: CH4 retrievals from space-based solar backscatter measurements: Performance evaluation against simulated aerosol and cirrus loaded scenes, J. Geophys. Res., 115, D24302, doi:10.1029/2010JD014514, 2010.

Butz et al., 2011: Butz, A., Guerlet, S., Hasekamp, O., et al., Toward accurate CO_2 and CH_4 observations from GOSAT, *Geophys. Res. Lett.*, doi:10.1029/2011GL047888, 2011.

Butz et al., 2012: Butz, A., Galli, A., Hasekamp, O., Landgraf, J., Tol, P., and Aben, I.: Remote Sensing of Environment, TROPOMI aboard Sentinel-5 Precursor : Prospective performance of CH_4 retrievals for aerosol and cirrus loaded atmospheres, 120, 267-276, doi:10.1016/j.rse.2011.05.030, 2012.

Butz et al., 2013: Butz, A. , Guerlet, S., Hasekamp, O.P., Kuze, A., and Suto, H. Using ocean-glint scattered sunlight as a diagnostic tool for satellite remote sensing of greenhouse gases. 2013. Atmos. Meas. Tech., 6, 2509.

Coddington et al. 2021: Coddington O. M., Richard, E. C., Harber, D., Pilewskie, P., Woods, T. N., Chance, K., et al. (2021). The TSIS-1 Hybrid Solar Reference Spectrum. *Geophysical Research Letters*, 48, e2020GL091709. https://doi.org/10.1029/2020GL091709

Van Diedenhoven et al., 2006: Van Diedenhoven, B., O.P. Hasekamp, and J. Landgraf, 2006: Efficient vector radiative transfer calculations in vertically inhomogeneous cloudy atmospheres. *Appl. Opt.*, **45**, 5993-6006.

Dubovik et al., 2006: Dubovik O., Sinyuk A., Lapyonok T., Holben B. N., Mishchenko M., Yang P., Eck T. F., Volten H., Muñoz O., Veihelmann B., van der Zande W. J., Leon J.-F., Sorokin M., Slutsker I. 2006. Application of spheroid models to account for aerosol particle nonsphericity in remote sensing of desert dust. J. Geophys. Res. D 111, D11208.

Duan et al., 2005: Minzheng Duan and Qilong Min. 2005. A fast radiative transfer model for simulating high-resolution absorption bands. J Geophys. Res. D 110, D15201.

Guerlet et al., 2013: Guerlet, S., A. Butz, D. Schepers, S. Basu, O. P. Hasekamp, A. Kuze, T. Yokota, J.-F. Blavier, N. M. Deutscher, D. W. T. Griffith, F. Hase, E. Kyro, I. Morino, V. Sherlock, R. Sussmann, A. Galli and I. Aben (2013) Impact of aerosol and thin cirrus on retrieving and validating XCO2 from GOSAT shortwave infrared measurements, J. Geophys. Res., doi: 10.1002/jgrd.50332

De Haan et al., 1987: de Haan, J. F., Bosma, P. B., Hovenier, J. W. (1987), The adding method for multiple scattering calculations of polarized light, Astron. and Astrophys., 183, 371 – 391.

Hansen, J.E., and L.D. Travis, 1974: Light scattering in planetary atmospheres. *Space Sci. Rev.*, 16, 527-610.

Hasekamp et al., 2002: Hasekamp, O. P. and Landgraf, J. (2002), A linearized vector radiative transfer model for atmospheric trace gas retrieval, J. Quant. Spectrosc. Radiat. Transfer, 75, 221–238.

Hasekamp et al., 2005a: Hasekamp, O. P. and Landgraf, J. (2005a), Linearization of vector radiative transfer with respect to aerosol properties and its use in satellite remote sensing, J. Geophys. Res, 110, D04203.

Hasekamp et al., 2005b: Hasekamp, O. P. and Landgraf, J. (2005b), Retrieval of aerosol properties over the ocean from multispectral single-viewing-angle measurements of intensity and polarization: Retrieval approach, information content, and sensitivity study, J. Geophys. Res. 110, D20207.

Hasekamp and Butz, 2008: Hasekamp, O. P. and Butz, A. (2008), Efficient calculation of intensity and polarization spectra in vertically inhomogeneous scattering and absorbing atmospheres, J. Geophys. Res., 113, D20309.

Jenouvrier et al., 2007: Jenouvrier, A., Daumont, L., Régalia-Jarlot, L., Tyuterev, V. G., Carleer, M., Vandaele, A. C., Mikhailenko, S., Fally, S. (2007), Fourier transform measurements of water vapor line parameters in the 4200 – 6600 cm-1 region, J. Quant. Spectrosc. Ra., 105, 326 – 355.

Kuze et al., 2009: Kuze, A., Suto, H., Nakajima, M., and Hamazaki, T. (2009), Thermal and near infrared sensor for carbon observation Fourier-transform spectrometer on the Greenhouse Gases Observing Satellite for greenhouse gases monitoring, Appl. Opt., 48, 6716–6733, 2009.

Kuze et al., 2014: Kuze, A., Taylor, T., Kataoka, F., Bruegge, C., Crisp, D., Harada, M., Helmlinger, M., Inoue, M., Kawakami, S., Kikuchi, N., Mitomi, Y., Murooka, J., Naitoh, M., O'Brien, D., O'Dell, C., Ohyama, H., Pollock, H., Schwandner, F., Shiomi, K., Suto, H., Takeda, T., Tanaka, T., Urabe, T., Yokota, T., and Yoshida, Y. (2014), Long-term vicarious calibration of GOSAT short-wave sensors: techniques for error reduction and new estimates of radiometric degradation factors, IEEE T. Geosci. Remote, 52, 3991–4004, doi:10.1109/TGRS.2013.2278696, 2014.

Kuze et al., 2016: Kuze, A., Suto, H., Shiomi, K., Kawakami, S., Tanaka, M., Ueda, Y., Deguchi, A., Yoshida, J., Yamamoto, Y., Kataoka, F., Taylor, T. E., and Buijs, H. L.: Update on GOSAT TANSO-FTS performance, operations, and data products after more than 6 years in space, Atmos. Meas. Tech., 9, 2445-2461, doi:10.5194/amt-9-2445-2016, 2016.

Landgraf et al., 2001: Landgraf, J., O. Hasekamp, T. Trautmann, and M. Box (2001), A linearized radiative transfer model for ozone profile retrieval using the analytical forward-adjoint perturbation theory, J. Geophys. Res., 106, 27,291 – 27,306.

Landgraf et al., 2002: Landgraf, J., O. Hasekamp, and T. Trautmann (2002), Linearization of radiative transfer with respect to surface properties, J. Quant. Spectrosc. Radiat. Transfer, 72, 327– 339.

Landgraf et al., 2009: Landgraf, J., Tol, P., Butz, A., Hasekamp, O., Aben, I. (2009), Level 1-B requirements for the SWIR 1.6 mm and 2.3 mm band, Camelot report, SRON/EOS/RP/09-005, SRON-Utrecht, The Netherlands.

Landgraf et al., 2010: Landgraf Jochen, Paul Tol, Otto P. Hasekamp, "Spatial Re-Sampling of Spectral Radiance Measurements of the O2 A-Band", Technote SRON-TROPSC-TN-2010-014, Netherlands Institute for Space Research (SRON), Utrecht, The Netherlands, 2010

Laughner et al., 2021: Laughner, J., Andrews, A., Roche, S., Kiel, M., and Toon, G. ginput v1.0.10: GGG2020 prior profile software (Version 1.0.10), https://doi.org/10.22002/D1.1944, 2021.

Mishchenko et al., 1999: Mishchenko, M. I., Geogdzhayev, I. V. , Cairns, B., Rossow, W. B., Lacis, A. A. (1999), Aerosol retrievals over the ocean using channel 1 and 2 AVHRR data: A sensitivity analysis and preliminary results, Appl. Opt., 38, 7325 – 7341.

Nakajima et al., 2017: M. Nakajima, Hiroshi Suto, K. Yotsumoto, K. Shiomi, T. Hirabayashi, "Fourier transform spectrometer on GOSAT and GOSAT-2," Proc. SPIE 10563, International Conference on Space Optics — ICSO 2014, 105634O (17 November 2017); https://doi.org/10.1117/12.2304062.

O'Brien et al. 2013: O'Brien, CJ, Peloquin, JA, Vogt, M, Heinle, M, Gruber, N, Ajani, P, Andruleit, H, Arístegui, J, Beaufort, L, Estrada, M, Karentz, D, Kopczyńska, E, Lee, R, Poulton, AJ, Pritchard, T, and Widdicombe, C. Global marine plankton functional type biomass distributions: coccolithophores. Earth Syst. Sci. Data, 5, 259-276, 2013 doi:10.5194/essd-5-259-2013

Peters et al., 2007: Peters, Wouter and Jacobson, Andrew R. and Sweeney, Colm and Andrews, Arlyn E. and Conway, Thomas J. and Masarie, Kenneth and Miller, John B. and Bruhwiler, Lori M. P. and Pétron, Gabrielle and Hirsch, Adam I. and Worthy, Douglas E. J. and van der Werf, Guido R. and Randerson, James T. and Wennberg, Paul O. and Krol, Maarten C. and Tans, Pieter P.: An atmospheric perspective on North American carbon dioxide exchange: CarbonTracker, PNAS, 104, 48, doi: 10.1073/pnas.0708986104

Philips, 1962: Phillips, D.L. (1962), A technique for the numerical solution of certain integral equations of the first kind, J. Assoc. Comput. Mach., 9, 84 – 97.

Rodgers, 2000: Rodgers, C.D. (2000), Inverse methods for atmospheric sounding: Theory and practice, World Sc., River Edge, USA.

Rodgers & Connors, 2003: Rodgers, C. D., and B. J. Connor (2003), Intercomparison of remote sounding instruments, J. Geophys. Res., 108, 4116, doi:10.1029/2002JD002299, D3.

Rothman et al., 2009: Rothman, L. S., Gordon, I. E., Barbe, A., Benner, D. C., Bernath, P. F., Birk, M., Boudon, V., Brown, L. R., Campargue, A., Champion, J. P., et al. (2009), The HITRAN 2008 molecular spectroscopic database, J. Quant. Spectrosc. Ra., 110, 533 – 572.

Scheepmaker et al., 2012: Scheepmaker, R. A., Frankenberg, C., Galli, A., Schrijver, H., Fally, S., Deutscher, N. M., Wunch, D., Warneke, T., Aben, I. (2012), Improved water vapour spectroscopy in the 4174 – 4300 cm-1 region and its impact on SCIAMACHY's HDO/ H2O measurements, Atmos. Meas. Tech., in preparation.

Schepers et al., 2012: Schepers, D., et al. (2012), Methane retrievals from Greenhouse Gases Observing Satellite (GOSAT) shortwave infrared measurements: Performance comparison of proxy and physics retrieval algorithms, J. Geophys. Res., 117, D10307, doi:10.1029/2012JD017549.

Stier et al., 2005: Stier, P., Feichter, J., Kinne, S., Kloster, S., Vignati, E., Wilson, J., Ganzeveld, L., Tegen, I., Werner, M., Balkanski, Y., Schulz, M., Boucher, O., Minikin, A., Petzold, A. (2005), The aerosol-climate model ECHAM5-HAM, Atmos. Chem. Phys., 5, 1125 – 1156.

Tikhonov et al., 1963: Tikhonov, A. (1963), On the solution of incorrectly stated problems and a method of regularization, Dokl., Akad., Nauk SSSR, 151, 501-504.

Tran et al., 2006: Tran, H., Boulet, C., Hartmann, J. M. (2006), Line mixing and collision-induced absorption by oxygen in the A band: Laboratory measurements, model, and tools for atmospheric spectra computations, J. Geophys. Res., 111, D15210.

Wunch et al. 2010: Wunch, D., Toon, G. C., Wennberg, P. O., Wofsy, S. C., Stephens, B. B., Fischer, M. L., Uchino, O., Abshire, J. B., Bernath, P., Biraud, S. C., Blavier, J.-F. L., Boone, C., Bowman, K. P., Browell, E. V., Campos, T., Connor, B. J., Daube, B. C., Deutscher, N. M., Diao, M., Elkins, J. W., Gerbig, C., Gottlieb, E., Griffith, D. W. T., Hurst, D. F., Jiménez, R., Keppel-Aleks, G., Kort, E. A., Macatangay, R., Machida, T., Matsueda, H., Moore, F., Morino, I., Park, S., Robinson, J., Roehl, C. M., Sawa, Y., Sherlock, V., Sweeney, C., Tanaka, T., and Zondlo, M. A.: Calibration of the Total Carbon Column Observing Network using aircraft profile data, Atmospheric Measurement Techniques, 3, 1351–1362, doi:10.5194/amt-3-1351-2010, URL http://www.atmos-meas-tech.net/3/1351/2010/, 2010.

Wunch et al. 2011: Wunch, D., Toon, G. C., Blavier, J.-F. L., Washenfelder, R. A., Notholt, J., Connor, B. J., Griffith, D. W. T., Sherlock, V., and Wennberg, P. O.: The Total Carbon Column Observing Network (TCCON), Philosophical Transactions of the Royal Society of London, Series A: Mathematical, Physical and Engineering Sciences, 369, 2087–2112, doi:10.1098/rsta.2010.0240, 2011.

Wunch et al. 2015: Wunch, D., Toon, G.C., Sherlock, V., Deutscher, N.M., Liu, X., Feist, D.G., Wennberg, P.O., The Total Carbon Column Observing Network's GGG2014 Data Version. Carbon Dioxide Information Analysis Center, Oak Ridge National Laboratory, Oak Ridge, Tennessee, USA, 2015.

Copernicus Climate Change Service

ECMWF - Shinfield Park, Reading RG2 9AX, UK

Contact: https://support.ecmwf.int/